Image watermarking with a directed periodic pattern to embed multibit messages resilient to print-scan and compound attacks

A. Keskinarkaus[*], A. Pramila[1], T. Seppänen[2]

P.O. Box 4500, 4STOCSE, FI-90014 University of Oulu, Finland

ABSTRACT

In this paper, we propose a blind method to embed multibit watermarks in images, robust to various attacks on geometry and print-scan process. For carrying the multibit information, a method using directed watermark patterns is proposed. A message sequence is mapped to a directional angle of a periodic pattern, which is then embedded into image blocks. In the detection, using autocorrelation function, filtering, masking, and adaptive line search with Hough transform, the alignment of the autocorrelations peaks are detected from image blocks, and interpreted as a message. The method provides a robust and blind extraction of information after a print-scan attack. Additionally, the experiments with two laser printer and two printout material show that the method is robust to compound attacks, such as Stirmark random bending, shearing, aspect ratio change, cropping, translation, or JPEG combined with print-scan.

1. Introduction

The confirmation of origin, integrity of content or tracing up forgery attempts is of growing importance. Different techniques can be considered when talking about protecting content. Watermarking is one of these techniques. The ease of copying images with printer and scanner has left a need for print-scan resilient watermarking techniques.

Printing and scanning inflict various attacks on the watermarked images such as DA/AD transform, noise addition, and geometrical attacks that are highly user dependent. Solanki et al. (2004, 2006) utilized experimental channel modeling, and proposed a method to estimate and undo rotation. The method is based on halftoning, which produces peaks to the magnitudes of the Fourier domain, and with these peaks, the rotation angle can be determined. He and Sun (2005) studied the print-scan process and proposed a scheme which uses image division into blocks. Fourier domain method was used to watermark textured blocks and spatial domain on smooth blocks to increase the capacity.

The geometrical distortions are usually considered as the most severe attacks in the print-scan process. Examples of proposed watermarking methods include invariant domain, such as the log-polar transform-based method proposed by Pereira and Pun (1999), binding the signature to image content using salient points, as proposed by Bas et al. (2002), and methods relying on synchronization patterns like methods proposed by Kutter (1998), Deguillaume et al. (2002), and Chen et al. (2006).

When a watermark is embedded multiple times in shifted locations in the image, an autocorrelation function can be used to indicate the amount of rotation and scaling. The methods by Deguillaume et al. (2002) and Kutter (1998) used this to embed self-referencing watermarks in images. Deguillaume et al. (2002) used a higher amount of repetitions, and consequently Hough transform and Radon transform, to extract the alignment of the autocorrelation peaks. Chen et al. (2006) arrived at a similar proposition as Deguillaume et al. (2002), but instead of one self-referencing watermark, they embedded two watermarks in the image: a periodic watermark for reference and a non-periodic watermark message based on modulation of the message sequences.

The autocorrelation function, in which the peak maximum is always located at the center, does not give information about the location of the watermark. As a result previously proposed methods (Kutter, 1998; Deguillaume et al., 2002; Chen et al., 2006; Keskinarkaus et al., 2006) use some auxiliary method such as edge detection, full search, or correlation to locate the watermarked area, prior to extracting the message or detecting the watermark. Accordingly these methods rely on the accuracy of the inversion process and restoring the image as well as possible prior to extraction/detection.

In this paper, a new method to utilize the periodic pattern is introduced. To embed a multibit message, the cover image is divided into blocks. One block carries reference information to indi-

* Corresponding author. Tel.: +358 405833116; fax: +358 8 5532534.
E-mail addresses: anja.keskinarkaus@oulu.fi, Anja.Keskinarkaus@ee.oulu.fi (A. Keskinarkaus), anu.pramila@oulu.fi (A. Pramila), tapio.seppanen@oulu.fi (T. Seppänen).
[1] Tel.: +358 407575686; fax: +358 8 5532534.
[2] Tel.: +358 8 5532897; fax: +358 8 5532534.

cate the amount of rotation and scaling the image has undergone. The other image blocks carry information, in which other periodic patterns, using different orientations are used to convey a multibit message in the modulated angle. The method extends the usage of a periodic pattern to carry a multibit message. Also, due to coding of the message as the direction of the periodic pattern, the additional synchronization search caused by translation and cropping can be avoided. Consequently, there is no need to use exhaustive search algorithms or edge detection. The proposed method is shown to be effective on compound effect of a fair amount of rotation, translation, cropping, and other distortions on geometry combined with a print-scan attack.

The paper is organized as follows: In Section 2, the theoretical background is explained with examples and an overview of the method is given. In Section 3, the method for embedding the messages is explained in detail and the message extraction process is described with the corresponding filtering, masking, and adaptive thresholding explained. In Section 4, in addition to capacity and imperceptuality considerations, we prove with experimental results the robustness of the proposed scheme to variety of attacks combined with the print-scan process. Finally, in Section 5, we discuss the related work and compare the obtained results to other print-scan resilient methods.

2. Detection of directed periodic patterns

A periodic pattern satisfies Eqs. (1) and (2)

$$W(x + q_0 N_0, y) = W(x, y); \quad q_0, N_0 > 1 \tag{1}$$

$$W(x, y + q_1 N_1) = W(x, y); \quad q_1, N_1 > 1, \tag{2}$$

where N_0 and N_1 determine the periodicity of repetitions, and q_0 and q_1 a repetition number on the horizontal and vertical directions. A periodic pattern exposes important properties. Firstly, the ACF (Autocorrelation function) $W*W$, referred as grid (G), reveals peaks (maximums) that are placed at grid intersections. Secondly, the peaks are equidistantly placed with respect to the fundamental periods (N_0, N_1). Finally, the orientation and fundamental periods are exposed to the same geometrical transforms as the actual image. Consequently, when a two dimensional watermark is embedded multiple times in shifted locations in the image, an autocorrelation function can be used to indicate the amount of rotation and scaling. Due to repetition, a large number of autocorrelation peaks survive, even under severe signal fading (Chen et al., 2006).

In Fig. 1a and b is shown an example in which a periodic watermark pattern, with a rectangular nature is placed to the luminance component over the whole Lena image. Due to periodicity, with autocorrelation, proper processing and thresholding, a small portion of the watermarked Lena image will be enough to reveal peak alignment. In the autocorrelation function, the number of periods that are visible is dependent on the size of the inspected area.

A previously nonutilized property in watermarking literature is that a directed grid $G^\theta = W^\theta * W^\theta$ has all the preceding properties, but it also keeps the information θ of the direction of the periodicity. We define a directed periodic pattern by

$$W^\theta = W(u', v') + \varepsilon = \Pi \left\{ \begin{bmatrix} \cos\theta & -\sin\theta \\ \sin\theta & \cos\theta \end{bmatrix} W(u, v) \right\}, \tag{3}$$

where $\prod$ defines the interpolation method and ε describes the error caused by interpolation. If a periodic 2D watermark pattern is rotated by θ and embedded to the image, we can similarly get information about the peak alignment from a small portion of image. Now however, the peaks tell about the orientation of the embedded pattern, as shown in Fig. 1c.

In Fig. 2 two even sized blocks of the Lena image contain a different periodic pattern (Fig. 2a and b). Illustration shows how shifting the window of inspection (Fig. 2c) does not reveal information of the translation, but the dominating orientation of the autocorrelation peak alignment is still recognizable (Fig. 2d). Similarly, if we slide the window so that background is cropped along, the alignment of peaks can be recovered. This is because regularity as in the periodic pattern does not exist in the background.

Based on the above considerations and examples, autocorrelation peak alignment is sustained well, although the window of inspection is not exactly in the right place or even of different size as the original. This is a property that is of disadvantage when considering methods, like (Kutter, 1998; Deguillaume et al., 2002; Chen

| (a) | (b) | (c) |
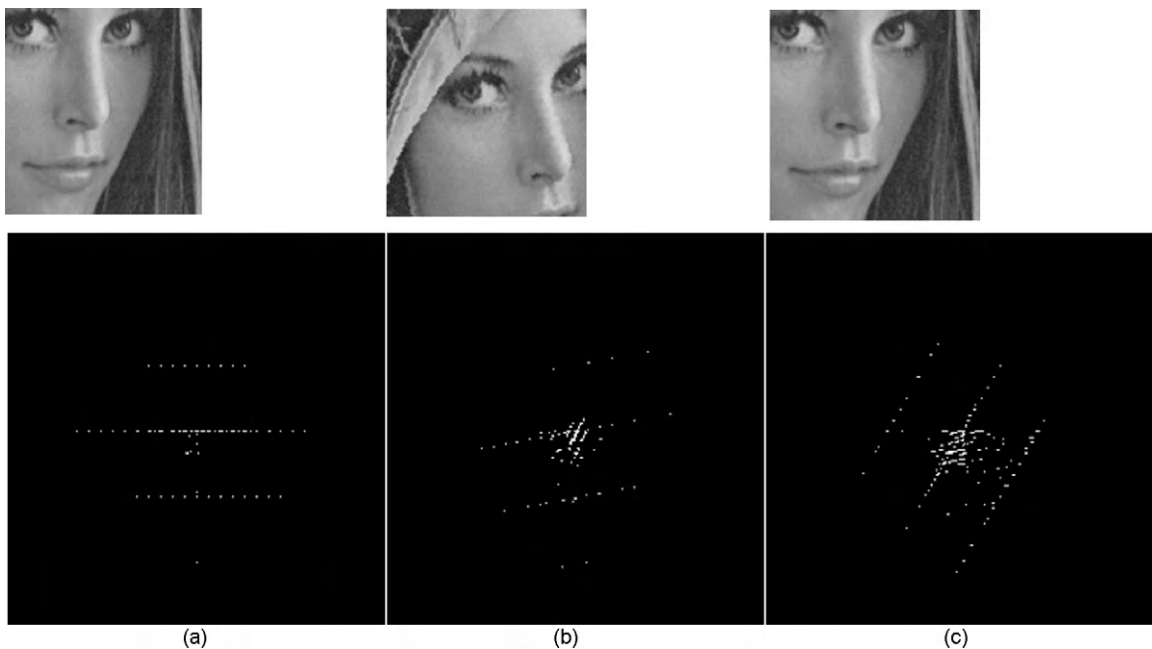
Fig. 1. (a and b) ACF of a small portion of Lena image will reveal information of the overall rotation of the image, when a watermark defined in Eqs. (1) and (2) is embedded. (c) The ACF peaks reveal information about the orientation of the embedded pattern, when a watermark defined in Eq. (3) is embedded ($\theta = 60°$).
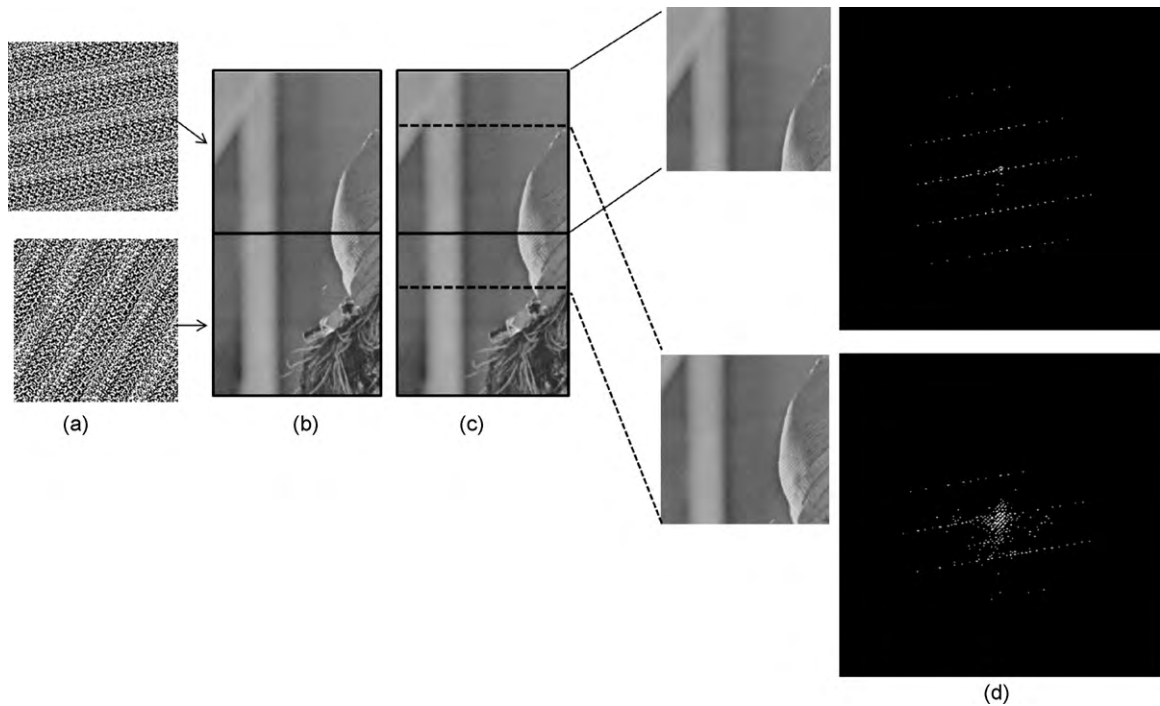
Fig. 2. (a) A directed periodic pattern with $\theta = 10°$ and $\theta = 60°$ generated using Eq. (3). (b) Two even sized blocks of the Lena image containing a different periodic pattern, upper block $\theta = 10°$ and lower block $\theta = 60°$. (c) The area of inspection shifted (dashed line). (d) Extracted autocorrelation peaks showing the effect of shifting the area of inspection.

et al., 2006; Keskinarkaus et al., 2006), in which actual location of the watermark has to be determined prior to detecting/decoding the message. However, those properties can be taken of advantage when watermarked images are printed and scanned and blind block division will differ from the original block division. Accordingly we propose a method to encode a message by modulating the θ of the periodic pattern. With such a periodic pattern direction of the range $\theta = [0° \ 180°[$ can be expressed assuming a reference coordinate frame exists.

A demonstration of the proposed method utilizing directed periodic patterns for watermarking is shown in Fig. 3. In this example

three bits per block are used for encoding directional data. The image is divided into blocks, 9 block division is used in this paper as an example. The luminance component of the image is utilized. One block is utilized to carry reference information and the other blocks carry information coded as the direction of the periodic pattern.

The flow of operations in the extraction process is shown in Fig. 4. Firstly an image is scanned from the context. The scanned image divided blindly to 9 blocks. Secondly, the reference block is used to detect and invert the overall rotation and scale (Fig. 4a). Hough transform is used to extract the alignment of the autocorrelation peaks. Additionally masking and adaptive thresholding, as
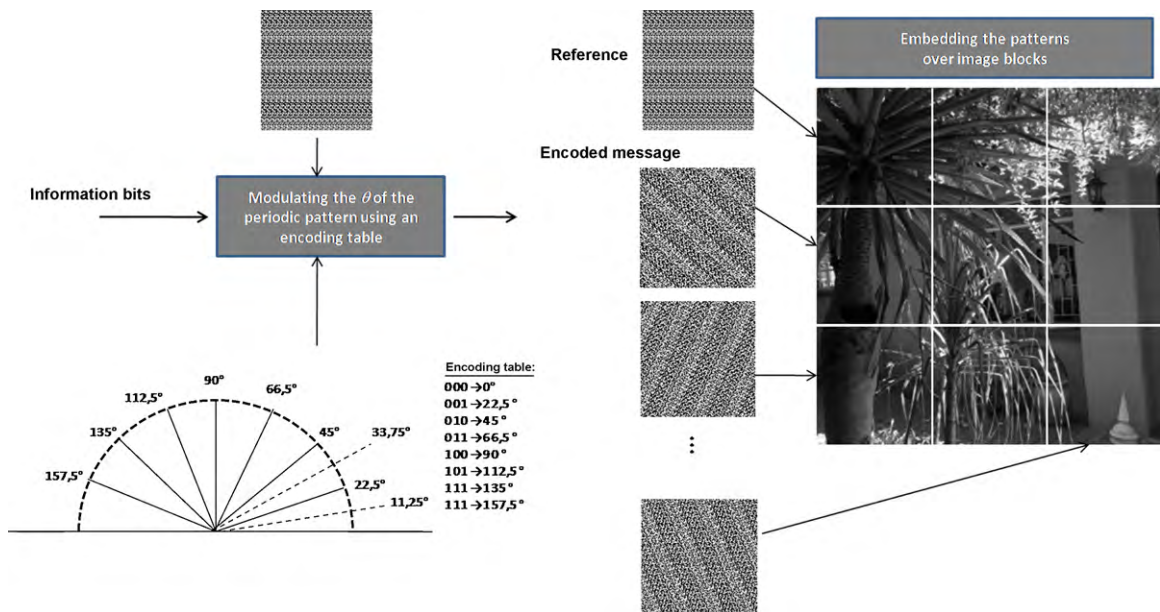
Fig. 3. Overview of the embedding process.
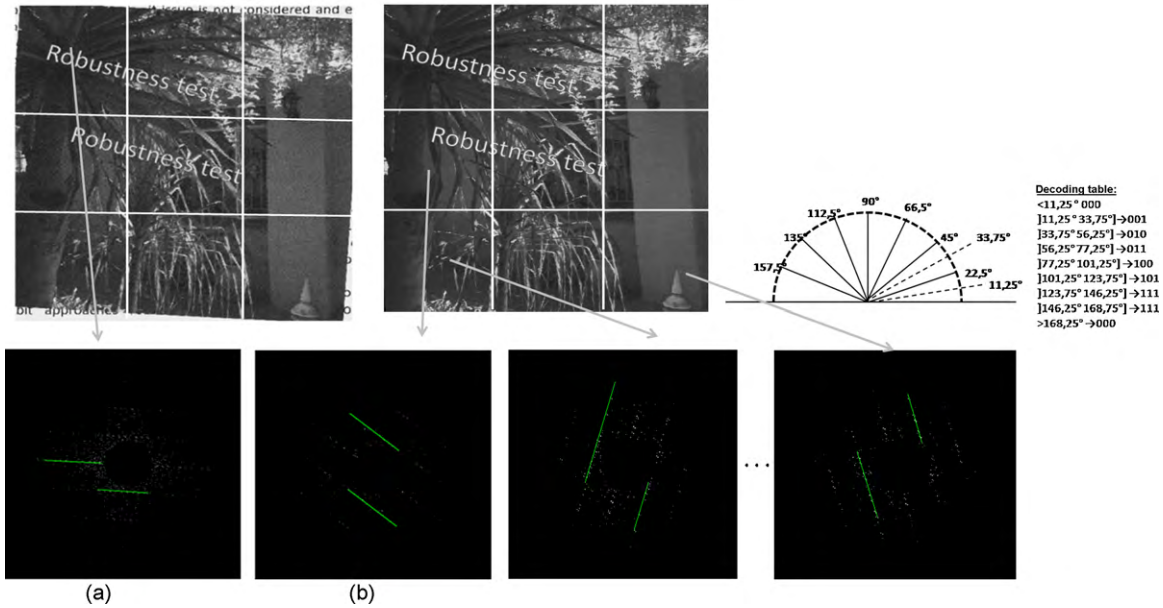
Fig. 4. Extraction of a multibit message from a scanned image. Information carried with the orientation of the directed grid used (a) to determine the overall rotation and scale from a reference block; (b) to determine the estimate of the angle in the information carrying blocks, to be interpreted as a message using the decoding table.

explained in Section 3, is utilized. After inversion the result image is divided to blocks again. Finally extraction of the message is realized by estimating the direction of the autocorrelation peaks from the message carrying blocks (Fig. 4b) and interpreting the message from the angle information using a decoding table. Method allows inaccuracy of the angle in detection, as a certain range of angle values will be interpreted similarly.

In the following sections, we explain give details about the embedding method, and explain the encoding of the message more formally and the extraction process in detail.

3. Watermark embedding and extraction

3.1. Watermark embedding

3.1.1. Encoding of the multibit message
Depending on the capacity requirements, the original message is divided into shorter messages m_i, where the message length $|m_i|$ expresses the amount of data bits that are to be embedded in the ith block of the image. The quantization step size is calculated with

$$\Delta = \frac{180}{2^{|m_i|}}, \tag{4}$$

where the constant 180 is defined by the range of θ. Thus far, uniform quantization is utilized. A codebook is derived accordingly. The message is expressed by mapping to the codebook values. Consequently, the original message is divided to be spread over the image blocks and represented by quantized orientation $Q_i(\theta)$.

3.1.2. Embedding a multibit message
The embedding of the message in the host image is realized in spatial domain utilizing the equation

$$Y_i^*(x, y) = X_i(x, y) + \lambda_1 \text{JND}_{fb} W_i^{Q(\theta_i)}(x, y), \tag{5}$$

where Y_i^* is ith watermarked block of the image, X_i is corresponding luminance component of the original image, $W_i^{Q(\theta_i)}$ is the directed periodic pattern, x and y describe the pixel position, JND_{fb} is the scaling factor attained from a JND profile, and λ_1 is an additional scaling factor.

The directed periodic pattern is generated utilizing Eq. (3) from pseudorandom values $\{-1,1\}$ to produce a rectangular, binary valued pattern. We use the nearest-neighbor method which produces values of $\{-1,1\}$, so there is no need for further thresholding to form the final binary valued pattern. Therefore, we can directly take advantage of the JND model.

The JND profile is calculated as explained in Chou and Li (1995), where the JND threshold is calculated for each pixel based on two properties of human eye, one of them being the average background luminance behind the pixel and the other the spatial uniformity of the background luminance. Fixed parameters settings, derived through visual experiments by Chou and Li (1995) are used to attain fidelity. The calculated full band JND profile is exploited for calculating a threshold for allowable distortion for every pixel value in an image. The model is the same utilized in our prior work (Keskinarkaus et al., 2006).

Print-scan process causes more distortion in highly textured image areas (see Fig. 13). In order to counter this, we evaluate the smoothness of the image area in 16×16 subblocks using average gradient magnitude on an image sharpened with an unsharp mask. We use linear relationship between λ_1 and the average gradient magnitude to place more watermark strength on textured blocks according to equation

$$\lambda_1 = \frac{\lambda_t - \lambda_s}{M_t - M_s} M_b + \lambda_s \tag{6}$$

In the Equation, λ_s is the scaling factor for smooth block and λ_t the scaling factor for textured block. M_s and M_t, respectively stand for average gradient magnitude on smooth and textured blocks. For λ_s, λ_t, M_s and M_t fixed values are used. The values are experimentally set by evaluating robustness vs. visibility on smooth and textured blocks, by measuring accuracy of angle detection together with overall BER and PSNR of the final outcome. M_b is the calculated average gradient magnitude of inspected 16×16 subblock and λ_1 the final watermark scaling factor used to watermark the inspected 16×16 subblock.

As a consequence of the layout of the watermarked image in the printing process or displacement of the image in the scanner bed, the overall rotation of the image is not known in advance. This causes the need for a reference coordinate frame. One of the blocks

serves as a carrier of the reference coordinate frame, angle $\theta = 0°$.

As an example, a 48 bit message 110110 011001 011101 110110 000101 100010 110010 011001, where $|m_i| = 6$ is embedded in the image. The image is divided into nine blocks. The message is then coded with a uniform quantizer, with $\Delta = 2.8125$, utilizing a codebook to message [153.2812°, 71.7188°, 82.9688°, 153.2812°, 15.4688°, 97.0312°, 142.0312°, 71.7188°]. Accordingly, we generate $W_i^{Q(\theta_i)}$, $i = 2, \ldots, 9$, where $Q(\theta)$ is equivalent to the coded message. $W_1^{0°}$ represents the reference coordinate frame and is embedded similarly. In our work, we used the upper left block for carrying reference information. Finally, the message is embedded using (5).

3.2. Watermark extraction

3.2.1. The extraction of information carried with the orientation of the directed grid

As during the embedding process, in the extraction process, the image is divided blindly into blocks. The number of blocks is the same as during embedding process, although due to print-scan process and other attacks, the size of the blocks will be different. A block division error is introduced, which depends on the combined effect of translation, cropping, and rotation, or another attack on geometry.

The message extraction process is based on the estimation of the orientation of peaks of the ACF. For each of the blocks, a Wiener estimate $\tilde{W}_i(x, y)$ of the periodic structure is calculated

$$\tilde{W}_i(x, y) = Y_i^*(x, y) - h(k) * Y_i^*(x, y), \tag{7}$$

where $Y_i^*(x, y)$ is the ith watermarked block, $h(k)$ represents the adaptive Wiener filtering. Autocorrelation function $R_{\tilde{W}_i, \tilde{W}_i}(u, v)$ is utilized in order to reveal the periodicity in the extracted watermark estimate

$$R_{\tilde{W}_i, \tilde{W}_i}(u, v) = \sum_x \sum_y \tilde{W}_i(x, y) \tilde{W}_i(x + u, y + v) \tag{8}$$

The autocorrelation is scaled to the range of [0,1],

$$R_{\tilde{W}_i, \tilde{W}_i}^*(u, v) = \frac{|R_{\tilde{W}_i, \tilde{W}_i}(u, v)|}{\max(R_{\tilde{W}_i, \tilde{W}_i}(u, v))} \tag{9}$$

Gradient operator (Sobel) is used to enhance the sharpness of the peaks. Filtering operation showed to be an effective and fast method to improve the distinguishing of peaks

$$R_{\tilde{W}_i, \tilde{W}_i}^{**}(u, v) = h_s(k) * R_{\tilde{W}_i, \tilde{W}_i}^*(u, v), \tag{10}$$

where $h_s(k)$ represents the Sobel filtering kernel. A binary grid image $G^*(u, v)$ is generated

$$G^*(u, v) = \begin{cases} 1, & \text{when } M(u, v) \times R_{\tilde{W}_i, \tilde{W}_i}^{**}(u, v) \geq \gamma \\ 0, & \text{when } M(u, v) \times R_{\tilde{W}_i, \tilde{W}_i}^{**}(u, v) < \gamma \end{cases}, \tag{11}$$

where $M(u, v)$ denotes a masking operation and γ is a threshold. The direction of periodicity in the proposed method is determined by examining the line segments determined from the peaks in the Hough transform matrix using $G^*(u, v)$. The central area of grid contains noise, as shown in Fig. 5. The cause of the noise is errors in this line detection. In or to reduce the noise, we use a masker

$$M(u, v) = \begin{cases} 1, & (D - k)^2 = (u - u_0)^2 + (v - v_0)^2 \\ 0, & \text{otherwise} \end{cases}, \tag{12}$$

where D is the distance from the centre, the radius of the masker, k is a small constant, and (u_0, v_0) is the centre of the ACF. In the example shown in Fig. 5, $D = N_1$ and $k = 2$, values which are used for extracting information from the message carrying blocks. The masking area is drawn as a circle. Masking forces the first lines to
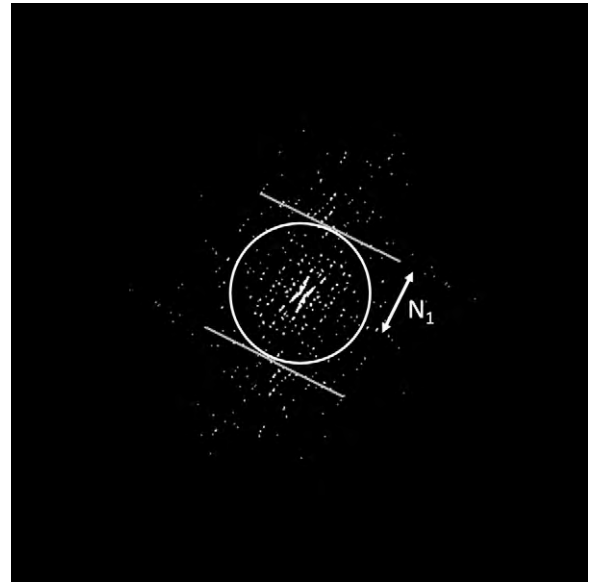

Fig. 5. Reducing false line detection using a circular mask defined with Eq. (12).

be detected just outside the circular area, and considerably reduces false line detection.

Due to the combined effect of affine transformations, other attacks and varying image content, γ cannot be fixed to be the same value for every ith block. Kutter (1998) suggested iterative approaches for synchronization search based on the number of extracted peaks. Based on our tests, the number of peaks does not give a proper estimate of γ when applied to different blocks in images. Therefore, we designed a new method to thresholding, which takes advantage of the fast operation of bare calculation of the number of peaks to give a rough estimate of the threshold, $\tilde{\gamma}$. Then the iterative call of Hough transform is used to find such a γ, that there are enough peaks for detecting lines exceeding a predetermined length. Alvarez-Rodríguez and Pérez-González (2002) discovered that the peak selection in template based synchronization affects the estimate of rotation. Through experiments, we came into alike conclusion: keeping the minimum length of lines fixed ensures that the accuracy of angle detection from lines is preserved.

Our adaptive approach proceeds as follows: The minimum length of the line segments, S, that are accepted as candidates for representing orientation angle, is fixed to L. The number of parallel lines that are searched for is also fixed. The following algorithm is looped while both of the search criteria are fulfilled. The threshold value is decreased using a small step size starting from the initial estimate, $\tilde{\gamma}$, as shown in Fig. 6. Now, from the extracted line segments, the estimate of the orientation of the directed grid $\tilde{\theta}$ can be determined for each of the blocks.

3.2.2. Interpreting the message

The search algorithm, described in the preceding section, is run first for the block containing the reference information. For the reference block, we use approximation $D = hC/(2q_0)$, where hC is horizontal dimension of ACF. Approximation is used as prior to evaluating the information from the reference block, scaling due to print-scan operation is not known. The result of running the algorithm for the reference block, gives the estimate of the overall rotation θ_r. In Fig. 7 it is illustrated that a fair estimate can be calculated from a small piece of original information.

After inverting the θ_r, projection of the grid against vertical axis gives the estimate of the scaling during print-scan process. We use the same procedure for calculating scaling as explained in Keskinarkaus et al. (2006).

```
flag=0;
r=;
while (flag==0)
    θ=∅;
    S=∅;
    S=Lines_Hough_Transform;
    for i=1:size(S)
        if (length(S[i])> L)
            Lines_accepted +=S[i];
        end
    end
    number_of_parallel_lines=number(round(θ(Lines_accepted)));
    if (number_of_parallel_lines <2)
        flag=0;
        r=r.r∆;
    else
        flag=1;
    end
end
```

Fig. 6. Adaptive line search algorithm for preserving the accuracy of the angle detection.

The extraction of the actual message proceeds block by block utilizing the same search algorithm. Due to calculation of the overall scaling, D is now known exactly. After inversion process, the message can be decoded from $\tilde{\theta}_k$ which is calculated utilizing $\tilde{\theta}_k = \tilde{\theta}_i - \theta_r^*$, where θ_r^* is calculated from the inverted image and is approximately zero. The message is decoded using the same quantization codebook as during embedding phase.

The accuracy of extracted orientations has to be in the range of $-\Delta/2 < \varepsilon(\theta) < \Delta/2$ in order to decode the message without errors. In other words, the accuracy of the angle detection has a direct effect on the capacity of the scheme. The smaller the $\varepsilon(\theta)$, the smaller Δ can be utilized, and consequently, more bits can be embedded in each block.
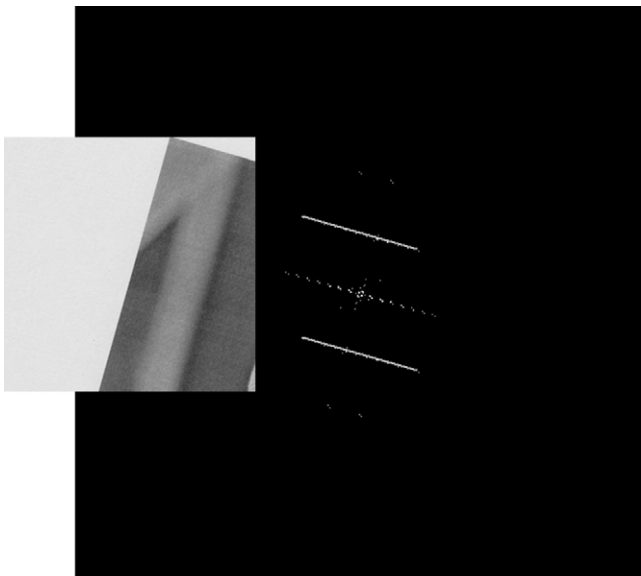

Fig. 7. Determining the overall rotation from the reference coordinate frame.
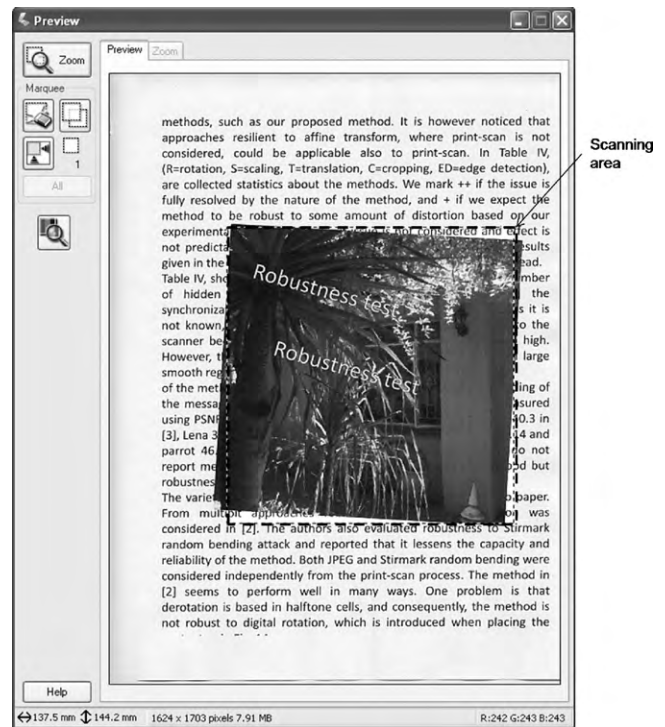

Fig. 8. EPSON photo scanner user interface, with the scanning area determination.

4. Experimental results

4.1. Application area and experimental setup

The process of watermarking the image, printing it, scanning the watermarked image and finally extracting or detecting the invisible message has been researched in (Solanki et al., 2004, 2006; He and Sun, 2005; Bas et al., 2002; Chen et al., 2006; Chiu and Tsai, 2006; Lin, 1999; Lefebvre et al., 2001; Lin and Chang, 1999; Hu, 2008). In these methods print-scan process has been considered as a separate attack and tests has been done from individual images printed on a white background. In here we widen the scope, to a realistic application case were the watermarked image exists in a printout such as document, a book or as a label adhered to product for copyright purposes or authentication. Consequently we require that the method should be robust to fair amount of layout processing and geometrical attacks caused by user interaction while determining the scanning area. Additionally, to offer a more general approach, the method should also be robust to background variation not relying on any edge detection methods. This is illustrated in Fig. 8 with an example.

The embedding and extraction algorithms were written in Matlab. There exists several brands of both scanner and printer technologies, with many intrinsic setting options. In here we used HP Color LaserJet 4650 PCL 6 and HP Color LaserJet 4700 PCL 6 printer and EPSON perfection, 4180 photo scanner. HP series printers represent current commercially available office laser printer technology, with high quality printouts and adaptive halftoning. We used of 600x600 dpi printing resolution and default settings of the printer. Scanning resolution of 300 dpi was used.

The parameters of the embedding and extraction were fixed. During embedding, we use $\lambda_s = 0.65$ for smooth blocks and $\lambda_t = 2.0$ for textured blocks Eq. (6). The corresponding values of M_s and M_t are 18 and 180. The extraction parameters were fixed, including the Hough transform parameters. The rectangular periodic pattern of pseudorandom values of $\{-1,1\}$, with $N_0 = 8$, $N_1 = 42$, $q_0 = 4$ and $q_1 = 22$ was used. For the search criteria, the length of the searched
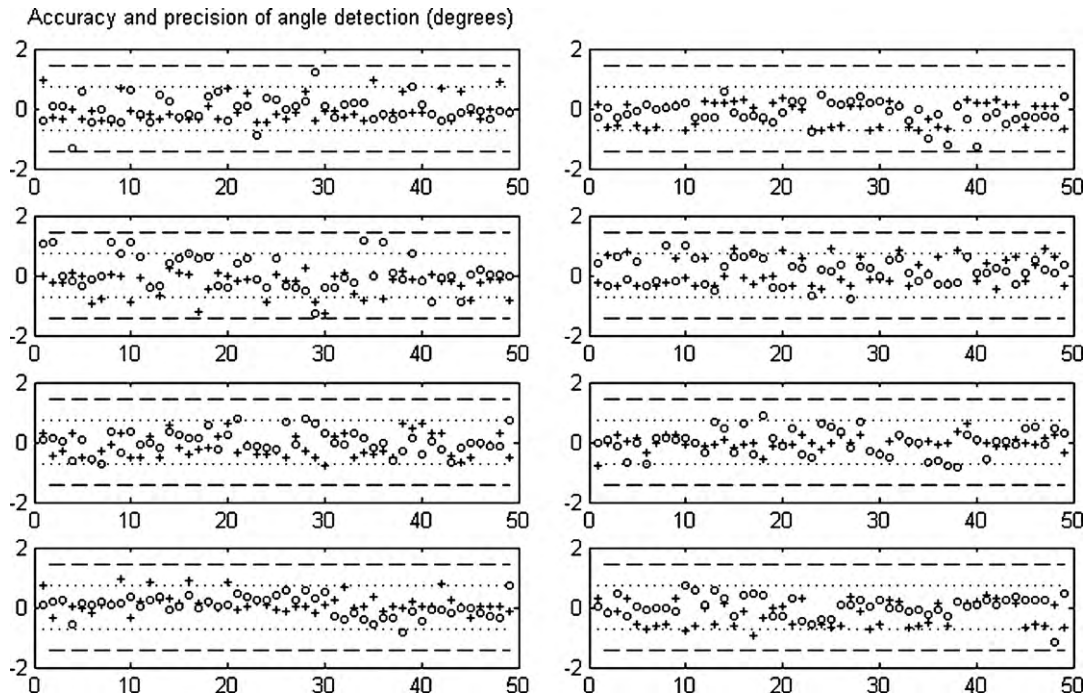
Fig. 9. Accuracy and precision of the angle detection over blocks in image. ('o') white background, normal office Xerox paper and HP Color LaserJet 4650 PCL 6, ('+') background varied, HP Color LaserJet 4700 PCL 6 Arron laser label material. Black dashed line ('- -') representing boundaries for capacity of 7 bits/block and dashed line('— —') 6 bits/block.

lines, L was set to be $hC/q_0 + 1$. Both of these choices decrease the amount of orthogonal errors while determining the angle. The number of parallel lines searched for, was set to be 2.

4.2. Angle detection and capacity with background variation and the effect of printout material

In order to investigate the effect of printer, material and background, the precision of the angle detection was measured with Lena image. In Fig. 9, eight subfigures represent the block number i, x-axel represents the individual test number, as the image is scanned repeatedly by varying the placement on the scanner bed.

In Fig. 9 we illustrate that regardless of the block in the image, background and with two printers and printout materials, the precision of the angle stays well within boundaries for carrying 6 bits/block. In that case, $|\varepsilon(\theta_k)|$ has to be <1.406°, expressed as dashed line('— —') in the figure. This indicates also that the proposed adaptive approach to thresholding works efficiently.

4.3. Robustness to print-scan compound with other attacks

Based on the previous results, the capacity of the method with the chosen settings, robust to general print-scan process, is 48 bits. In the following we inspected how a combination of attacks effects on the capacity. The tests were realized with 16 images, size of 510×510, shown in Fig. 10. The proposed method can be similarly used for images of other size. We embedded 48 (6 bits/block), 40 (5 bits/block) and 32 (4 bits/block) bits to the 16 test images and measured the invisibility and robustness of the method.

In Tables 1 and 2, first row, columns 4–11 present the combination of attacks tested. The numerical value in the next rows expresses how much additional attack, besides printing and scanning, the watermarked test image tolerates. As an example, additionally to print-scan operation, the 40 bit message extraction (Table 2) from im4 is robust if rotation is $\leq \pm 10$ or cropping of image is $\leq 8\%$. Considering the attack is no stronger than expressed in Table 1 (6 bits/block), the success ratio of all inspections was 98.9% out of over 600 repetitions of the extraction process. When

Table 1
Limits for robust message extraction (6 bits/block).

im	wm	PSNR (dB)	PS+ rot (°)	PS + crop (%)	PS + AR change	PS + x_ shear (%)	PS + y_ shear (%)	JPEG (QF) + PS	PS + trans (%)	PS + scale (%)
im1	deer98	31.2	20	14	1:0.96	1	2	90	13	66
im2	bloom6	33.7	18	18	1:0.98	2	2	90	12	68
im3	hdr555	33.0	12	18	1:0.99	1	1	90	13	66
im4	sami5v	35.7	12	6	1:0.99	0.9	1	95	10	70
im5	niina7	35.8	22	24	1:0.96	2	2	95	13	68
im6	spider	36.8	18	22	1:0.98	1	2	95	15	80
im7	zebra1	29.5	20	18	1:0.98	1	2	90	15	66
im8	confir	35.9	14	10	1:0.98	2	2	95	4	85
im9	buildi	30.4	18	16	1:0.99	1	2	90	13	68
im10	bigtre	29.1	12	14	1:0.98	1	2	90	13	70
im11	childre	35.1	12	6	1:0.98	2	2	90	11	68
im12	splash	35.6	20	8	1:0.98	2	2	90	10	68
im13	tiffan	36.9	20	20	1:0.98	2	1	95	8	68
im14	mandri	29.9	6	6	1:0.98	1	2	90	6	85
im15	lena12	35.1	14	14	1:0.99	1	0.8	95	5	75
im16	pepper	34.6	16	8	1:0.98	2	2	90	5	68

Fig. 10. Test images.

Table 2
Limits for robust message extraction (5 bits/block).

| im	wm	PSNR (dB)	PS + rot (°)	PS + crop (%)	PS + AR change	PS + x_ shear (%)	PS + y_ shear (%)	PS + x and y shear (%)	JPEG (QF) + PS	PS + trans (%)	PS + scale (%)
im1	deer9	31.2	14	12	1:0.94	3	3	2	90	12	72
im2	bloom	33.7	14	16	1:0.92	3	4	1	90	13	66
im3	hdr55	33.0	18	22	1:0.94	4	4	1	90	16	66
im4	sami5	35.7	10	8	1:0.92	5	5	3	95	8	68
im5	niina	35.8	10	16	1:0.94	3	4	1	95	16	70
im6	spide	36.8	20	16	1:0.92	3	4	3	95	10	68
im7	zebra	29.5	20	18	1:0.92	5	5	2	90	14	66
im8	confi	35.9	10	6	1:0.94	5	4	2	95	5	68
im9	build	30.4	18	28	1:0.92	5	5	2	90	13	64
im10	bigtr	29.1	10	16	1:0.92	4	4	1	90	12	68
im11	childr	35.1	18	16	1:0.92	3	2	2	90	12	72
im12	splas	35.6	20	20	1:0.92	5	5	2	90	7	68
im13	tiffa	36.9	22	18	1:0.90	4	5	2	95	16	70
im14	mandr	29.9	12	4	1:0.98	2	2	2	90	5	70
im15	lena1	35.2	20	14	1:0.90	4	5	2	95	11	66
im16	peppe	34.7	12	10	1:0.96	4	3	2	90	5	70
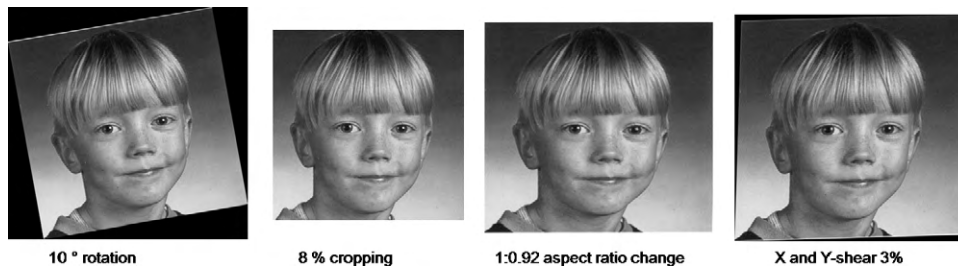
Fig. 11. Examples of attacked images (im4), 5 bits/block embedded (Table 2), extraction robust.

Table 3
The combined effect of stirmark random bending attack/local data removal and print-scan on message extraction reliability.

im	wm 5 bits/block	wm 4 bits/block	PS + Stirmark random bending (5bits/block) BER	PS + Stirmark random bending (4 bits/block) BER	wm 6 bits/block	PS + Local removal of block data (15% of block data removed) (6 bits/block) BER	PS + Local removal of reference block data (25% of block data removed) (6 bits/block) BER	PS + Local removal of block data (5% of block data removed) (6 bits/block) BER
im1	deer9	deer	0	0	deer98	0	0	0
im2	bloom	bloo	0	0	bloom6	0	0	0
im3	hdr55	hdr5	0	0	hdr555	0	0	0
im4	sami5	sami	0	0	sami5v	0	0	0
im5	niina	niin	0	0	niina7	0	0	0
im6	spide	spid	0	0	spider	0	0	0
im7	zebra	zebr	0.025	0	zebra1	0	0	0
im8	confi	conf	0.025	0	confir	0	0	0
im9	build	buil	0.075	0	buildi	0	0	0
im10	bigtr	bigt	0	0	bigtre	0	0	0
im11	childr	child	0.025	0	childre	0	0	0
im12	splas	spla	0.025	0	splash	0	0	0
im13	tiffa	tiff	0.075	0	tiffan	0	0	0
im14	mandr	mand	0.050	0	mandri	0	0	0
im15	lena1	lena	0	0	lena12	0	0	0
im16	peppe	pepp	0	0	pepper	0	0	0

not successful, 1 or 2 bit error was detected. No errors were detected when embedding 5 bits/block (Table 2).

Comparing the results in Tables 1 and 2, it can be seen that decreasing the number of bits/block increases the robustness to geometrical attacks, such as aspect ratio change, x_shear, y_shear and combined x_shear and y_shear. This is due to the fact that when embedding 6 bits/block, angle detection accuracy $|\varepsilon(\theta_k)|$ has to be <1.406° for robust extraction. When decreasing the amount of bits/block to 5, this requirement is relaxed to $|\varepsilon(\theta_k)| < 2.812°$, which allows the skew caused by non-uniform geometrical attacks. In order to illustrate the amount of allowed additional attacks, examples of im4 attacked, as indicated in Table 2, are shown in Fig. 11.

We tested the compound effect of Stirmark random bending attack (Petitcolas et al., 1998) and print scan attack. In the attack, non-uniform localized geometrical transforms are applied randomly to the image. The results of these inspections are collected in Table 3. The results showed that a 32 bit message can be reliably extracted from all the test images. Additionally we run experiments on local removal of watermark data. Tests showed that the method is fairly robust on those attacks. Examples of attacked images are shown in Fig. 12 and test results are presented in Table 3.

4.4. Quality of the watermarked images

For quality evaluation, in Fig. 13 is shown an example image watermarked with 48 bits (6 bits/block). Measured PSNR values are depicted in Tables 1 and 2.
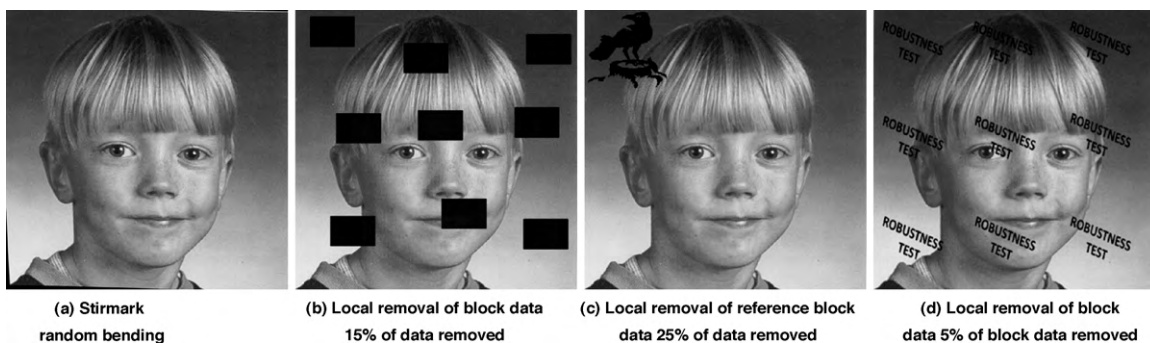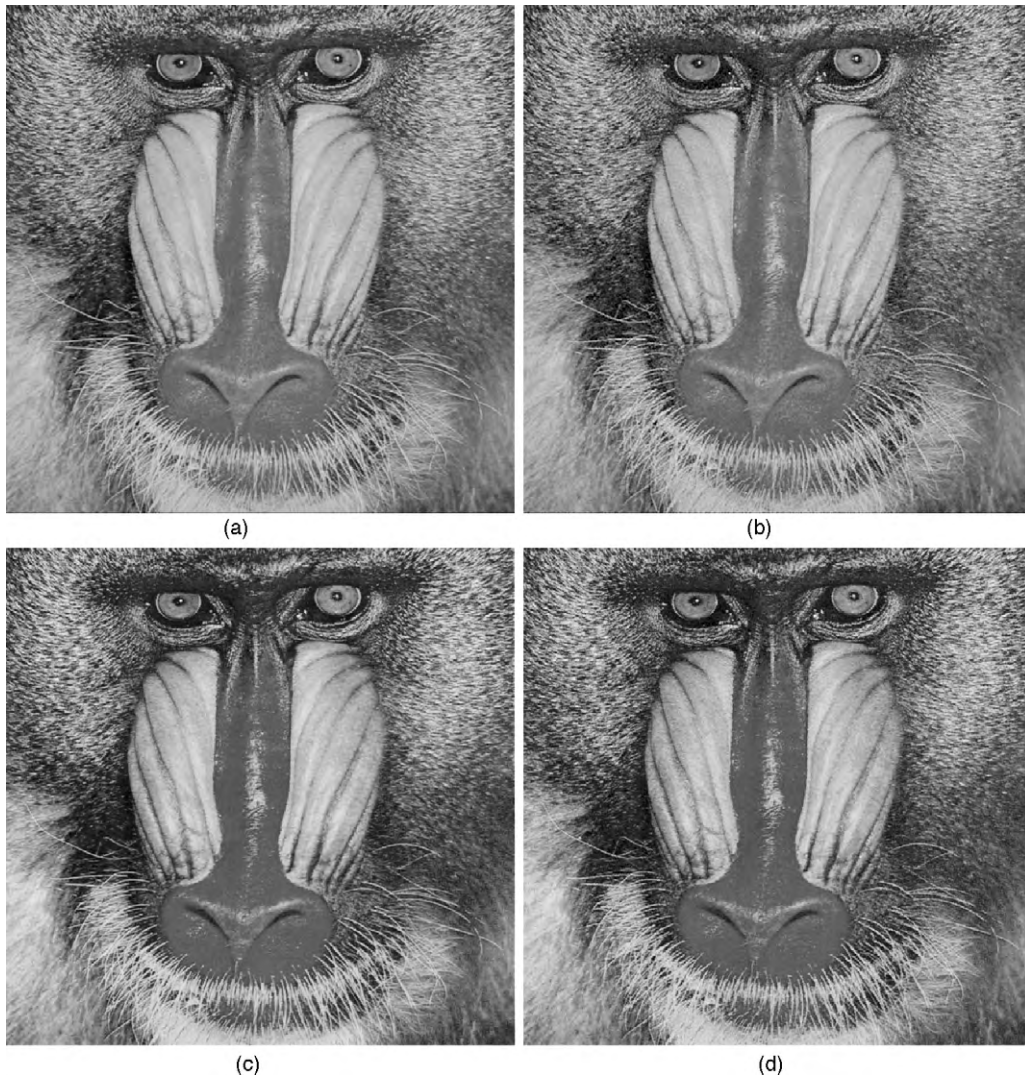

Fig. 12. Examples of attacked images (im4), (a) 4 bits/block, attacked with PS + Stirmark random bending (b), (c) and (d) 6 bits/block embedded, attacked with PS+data removal.

Fig. 13. (a) Original Baboon image, (b) watermarked baboon image (6bits/block), (c) printed and scanned original image, and (d) printed and scanned watermarked image.

Table 4
Comparison table (ED = edge detection).

	Synchronization	Multibit Y/N
Proposed method	Directed periodic pattern	Y (48/40 bits)
Solanki et al. (2004, 2006)	Halftone cells + ED	Y (few hundred bits)
He and Sun (2005)	ED	Y (1024 bits)
Bas et al. (2002)	Salient points	N
Chen et al. (2006)	Spatial template + ED	Y (64 bits)
Chiu and Tsai (2006)	Frequency domain peak	Y (serial number 888)
Lin (1999)	Log–log mapping	Y(14*3 bits)/N
Lefebvre et al. (2001)	Frequency domain template	Y
Lin and Chang (1999)	Invariant features	N
Hu (2008)	Feature points	Y(~20bits)[a]

[a] The authors do not report the capacity, so an estimate for Lena image was calculated from Fig. 4 in Hu (2008).

5. Discussion and conclusion

In addition to geometrical distortions, printer/scanner optical and mechanical distortions are challenging. Every time an image is printed and scanned, even with proper placement of the paper into the scanner bed, the result image is different (Yu et al., 2005). This difference, although barely visible to eyes, makes a difference when extracting the message or detecting the existence of a watermark compared to message extraction/detection without print-scan attack. As a result, the comparison of the proposed method was done against methods where print-scan attack is considered (see Table 4 for references). All of these are blind methods, such as our proposed method. It is however noticed that some of the approaches resilient to affine transform (Pereira and Pun, 1999; Kutter, 1998; Deguillaume et al., 2002; Zhang and Xin, 2009; Dainaka et al., 2006; Fung and Kunisa, 2005; Liu and Zhao, 2004), might be applicable also to print-scan. Also in here we do not consider halftone-based methods, which are based in direct manipulation of halftone cells, like method proposed by Xu and Wan (2008).

Some of the methods are multibit methods, requiring the correct decoding of the message. From Table 4 can be seen that most of those rely on some edge detection method. In Lin (1999) the robustness results for multibit message to print-scan attack are not provided. In He and Sun (2005) the number of hidden bits is bigger than in other methods. Authors however report an increase in BER, when the reading of the watermark is not accurately synchronized.

Compound effect of print-scan and other attacks has not been studied in the papers. The variety of other attacks considered, changes from paper to paper. From multibit approaches, robustness to JPEG compression and Stirmark random bending attack was considered in Solanki et al. (2006) and Hu (2008). In Solanki et al.

(2006), the authors reported that random bending attack lessens the capacity and reliability of the method. The method in Solanki et al. (2006), seems to perform well in many ways. One problem is that derotation is based in halftone cells, and consequently, the method is not robust to digital rotation. In Hu (2008) the method is not robust to aspect ratio changes, but performs well against many other attacks on geometry.

The proposed method is proven to be robust to compound effect of print-scan and attacks on geometry. Adaptive approach resolves difficult issues, like proper thresholding, and consequently, independent watermarks can be extracted blindly without a change of parameters during extraction. Two printers and printout materials were tested to prove robustness. No edge detection method is needed, which we see as an advantage when the background of the image is other than uniformly colored. The runtime of nonoptimized matlab implementation using standard PC is only a few minutes, thus the proposed method is also computationally feasible.

References

Alvarez-Rodríguez, M., Pérez-González, F., 2002. Analysis of pilot-based synchronization algorithms for watermarking of still images. Signal Processing: Image Communication 17 (8), pp. 611-633.

Bas, P., Chassery, J.-M., Marq, B., 2002. Geometrically invariant watermarking using feature points. IEEE Transactions Image Processing 11, 1014–1028.

Chen, P., Zhao, Y., Pan, J.-S., 2006. Image watermarking robust to print and generation copy. In: 1st International Conference on Innovative Computing, Information and Control, vol. 1, ICICIC, pp. 496–500.

Chiu, Y.-C, Tsai, W.-H., 2006. Copyright protection against print-and-scan operations by watermarking for color images using coding and synchronization of peak locations in frequency domain. Journal of Information Science and Engineering 22 (3), 483–496.

Chou, D.-H., Li, Y.-C., 1995. A perceptually tuned subband image coder based on the measure of just-noticeable-distortion profile. IEEE Transactions on Circuits and Systems for Video Technology 5 (6), 467–476.

Dainaka, M., Nakayama, S., Echizen, I., Yoshiura, H., 2006. Dual-plane watermarking for color pictures immune to rotation, scale, translation, and random bending. In: International Conference on Intelligent Information Hiding and Multimedia Signal Processing (IIH-MSP'06), pp. 93–96.

Deguillaume, F., Voloshynovskiy, S., Pun, T., 2002. Method for the estimation and recovering from general affine transforms in digital watermarking applications. In: Proceedings of SPIE, Electronic Imaging, Security and Watermarking of Multimedia Contents IV, vol. 4675, pp. 313–322.

Fung, W.W.L., Kunisa, A., 2005. Rotation, scaling, and translation-invariant multi-bit watermarking based on log-polar mapping and discrete Fourier transform. In: IEEE International Conference on Multimedia and Expo, 4 pp. 141–144.

He, D., Sun, Q., 2005. A practical print-scan resilient watermarking scheme. In: IEEE International Conference on Image Processing (ICIP) 1, pp. I-257-60.

Hu, S., 2008. Geometric-invariant image watermarking by key-dependent triangulation. International Journal of Computing and Informatics 32 (2), 169–181.

Keskinarkaus, A., Pramila, A., Seppänen, T., Sauvola, J., 2006. Wavelet domain printscan and JPEG resilient data hiding method. In: Proceeding of 5th International Workshop on Digital Watermarking, vol. 4283, Jeju Island, Korea, LNCS, pp. 82–95.

Kutter, M., 1998. Watermarking resistant to translation, rotation and scaling. In: Proceedings of SPIE, Multimedia Systems and Applications, vol. 3528, Boston, MA, pp. 423-431.

Lefebvre, F., Gueleuy, D., Delanney, D., Macq, B., 2001. A print and scan optimized watermarking scheme. In: Proceedings of IEEE Fourth Workshop on Multimedia Signal Processing, pp. 511–516.

C.-Y. Lin, 1999. Public watermarking surviving general scaling and cropping: an application for print-scan process. Multimedia and Security Workshop at ACM Multimedia 99, Orlando, FL.

Lin, C.-Y., Chang, S.-F., 1999. Distortion modelling and invariant extraction for digital image print-scan process. In: International Symposium on Multimedia Information Processing (ISMIP 99), Taiwan.

Liu, Y., Zhao, J., 2004. Rotation, scaling, translation invariant image watermarking based on radon transform. In: 1st Canadian Conference on Computer and Robot Vision (CRV'04), pp. 225–232.

Pereira, S., Pun, T., 1999. Fast robust template matching for affine resistant image watermarking. In: International Workshop on Information Hiding, ser. Lecture Notes in Computer Science, vol. LNCS 1768. Springer-Verlag, Berlin, Germany, pp. 200–210.

Petitcolas, F., Anderson, R., Kuhn, M., 1998. Attacks on copyright marking systems. In: Information Hiding, Second International Workshop, IH'98, Portland, Oregon, U.S.A., Proceedings, LNCS 1525, Springer-Verlag, pp. 219–239.

Solanki, K., Madhow, U., Manjunath, B.S., Chandrasekaran, S., 2004. Estimating and undoing rotation for print-scan resilient data hiding. In: IEEE International Conference on Image Processing (ICIP), Oct. 24–26, vol. 1, pp. 39–42.

Solanki, K., Madhow, U., Manjunath, B.S., Chandrasekaran, S., El-Khalil, I., 2006. 'Print and scan' resilient data hiding in images. IEEE Transactions Information Forensics and Security 1 (4), 464–478.

Xu, H., Wan, X., 2008. Watermarking algorithm for print-scan based on HVS and multiscale error diffusion. In: International Conference on Computer Science and Software Engineering 6, 245–248.

Yu, L., Niu, X., Sun, S., 2005. Print-and-scan model and the watermarking countermeasure. Image and Vision Computing 23 (9), 807–814.

Zhang, X., Xin, L., 2009. A novel watermarking algorithm resist to geometrical attacks. In: International Conference on Electronic Commerce and Business Intelligence, pp. 503–506.

Anja Keskinarkaus received her M.Sc degree in Information Engineering in 1998 from the University of Oulu, Finland. Since 1997, he has been working at the University of Oulu as a researcher and project manager in numerous research projects. Her doctoral research subject is print-scan resilience of digital watermarking methods for images. Her research interests include digital watermarking of audio, speech and images, and mobile applications taking advantage of watermarking methods.

Anu Pramila is a Ph.D. student at the Department of Electrical and Information Engineering at the University of Oulu. She graduated with honors as Master of Science in Engineering at the University of Oulu in March 2007 with a thesis subject of "Watermark synchronization in camera phones and scanning devices." Currently, she works as research scientist at MediaTeam Oulu research group at the University of Oulu.

Tapio Seppänen (M'95) received his M.Sc. degree in Electrical Engineering in 1985 and the Ph.D. degree in computer engineering in 1990 from the University of Oulu, Finland. Currently he is serving as a full professor at the same university. He teaches and conducts research on multimedia signal processing and biomedical signal processing. Special interests include digital watermarking, pattern recognition applications, and processing of cardiovascular signals and EEG signals.